Short Papers

Electronic Throttle Valve Modeling Considering Nonlinearity of Electrical and Mechanical Parameters Based on Experiments

Jin-Cheol Park, Jun-Yeol Ryu, Soo-Hwan Park, and Myung-Seop Lim, *Member, IEEE*

***Abstract*—In this article, the nonlinear parameters of a throttle valve were analyzed and calculated to predict its dynamic characteristics. A mathematical model considering nonlinear parameters is employed to improve the control performance over the throttle valve. Electrical nonlinearity is caused by the brush and commutator. A brush contact resistance is generated due to the contact between the brush and commutator. The brush contact resistance is affected by the rotor speed and the input current. Furthermore, mechanical nonlinearity is caused by the limp-home mode in the spring. The torque produced by the spring varies with the valve angle. As it is difficult to estimate nonlinear parameters accurately, electrical and mechanical parameters were calculated experimentally. In addition, a block diagram considering the nonlinearity of the electrical and mechanical parameters was developed. Finally, the test and simulation results were compared to validate the estimated nonlinear parameters.**

***Index Terms*—Brushed dc motor, nonlinear parameter, throttle valve.**

I. Introduction

A THROTTLE valve is widely used in internal combustion engines and hybrid electric vehicles. The amount of air injected into the engine cylinder can be controlled using the throttle valve, allowing the vehicle to be accelerated or decelerated [1]. An adequate balance of acceleration and deceleration leads to an optimal condition for vehicle operation. To achieve stable engine operation and low gas emissions, high control performance is required by regulating the throttle valve. In addition, precise control of the throttle valve in next-generation vehicles equipped with features, such as vehicle-to-vehicle autonomous driving and cruise control, is required to ensure the efficient performance of such vehicles [2].

For the stability and high control performance of the throttle valve, a control design that considers the nonlinear parameters is required. The throttle valve includes nonlinear parameters owing to complex electrical and mechanical structures, such as brushed direct current (dc) motors, gears, and springs. Consequently, the prediction of the dynamic characteristics for the throttle valve becomes difficult owing to the nonlinear parameters. Several control techniques have been adopted to compensate for this inaccurate performance caused by nonlinear parameters; these techniques include sliding-mode control, adaptive control, and fuzzy theory based on proportional-integral-derivative (PID) control. A common method to control the throttle valve position is the feedback method using PID control and position sensors [3]. PID control is based on an integrated mathematical model of voltage and motion equations. Moreover, sliding mode control is commonly used to achieve control stability [4]–[6]. Adaptive control and fuzzy theory are used to compensate for positional changes resulting from system nonlinearities [7]–[9]. However, most of the previous studies have focused on control design considering mechanical nonlinearities, such as spring and gear backlash [10], [11]. To establish an accurate control strategy or design, it is necessary to consider both electrical and mechanical nonlinearity.

Fig. 1 illustrates the structure of a throttle valve system. The throttle valve is controlled by an accelerator pedal via a driver or vehicle control. Feedback control is performed using the plate and accelerator pedal position sensors to appropriately control the plate motion. The amount of air supplied to the engine is adjusted according to the plate motion. The throttle valve can be divided into electrical and mechanical components. The electrical component includes a brushed dc motor that converts electrical energy into mechanical energy. Nonlinearity in the electrical parameter is caused by the brush and commutator used to generate a constant torque. As the contact area between the brush and commutator depends on the rotor speed and current, it is difficult to predict brush performance [12]–[14]. Furthermore, the mechanical components include gears, the plate, and springs. The gears transmit the mechanical energy generated by the brushed dc motor to the plate. The spring determines the opening and closing of the plate position. Nonlinearity in the mechanical parameters is caused by the spring. Two springs exhibiting different performances are used to assist the opening and closing of the throttle valve. The section that balances the forces by two springs of different performance is called the limp-home [15], [16].

Most mathematical models and control designs consider only the nonlinearity of the mechanical parameter. However, neglecting the nonlinearity of the electrical parameter can lead to inaccurate predictions of the dynamic characteristics for the throttle valve performance.

The main contributions of this article are as follows:

1) A calculation process is presented for electrical and mechanical parameters with nonlinearity.
2) Mathematical modeling is proposed considering the nonlinearities in electrical and mechanical parameters.
3) The proposed model is validated through experiments.

Because the analytical calculation of the electrical and mechanical parameters is difficult owing to the complex structure of the throttle valve, the parameters are calculated experimentally.

Manuscript received 23 February 2021; revised 15 June 2021 and 4 September 2021; accepted 24 September 2021. Date of publication 16 November 2021; date of current version 17 October 2022. Recommended by Technical Editor J. Zhang. Senior Editor Y. Li. This work was supported by the National Research Foundation of Korea (NRF) funded by the Korea government (MSIT) under Grant NRF-2020R1A4A4079701. *(Corresponding author: Myung-Seop Lim.)*

The authors are with the Department of Automotive Engineering, Hanyang University, Seoul 04763, South Korea (e-mail: skensk1990@hanyang.ac.kr; jesus0925@hanyang.ac.kr; shwanp14@hanyang.ac.kr; myungseop@hanyang.ac.kr).

Color versions of one or more figures in this article are available at https://doi.org/10.1109/TMECH.2021.3123137.

Digital Object Identifier 10.1109/TMECH.2021.3123137

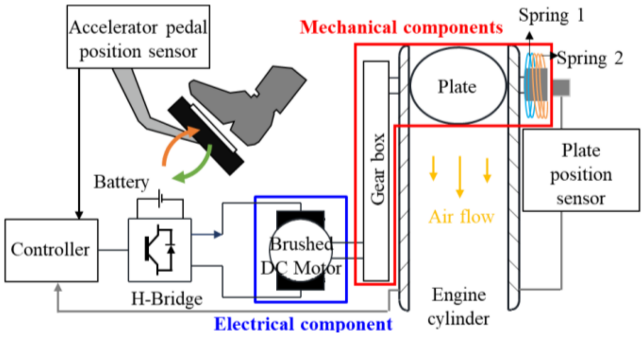

Fig. 1. Structure of a throttle valve system.

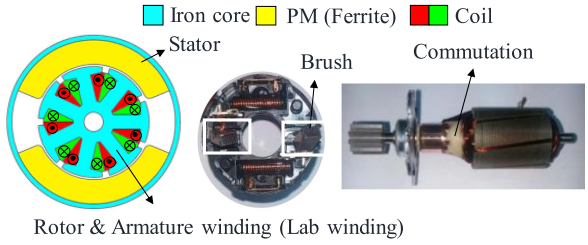

Fig. 2. Components of brushed dc motor: stator, rotor, brush, and commutator.

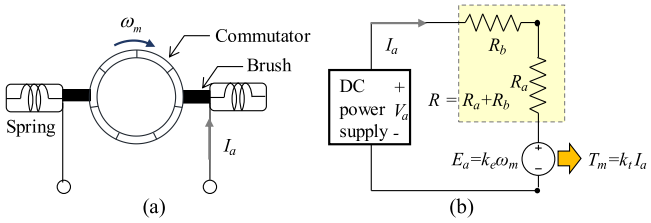

Fig. 3. Brushed dc motor. (a) Schematic of contact brush and commutator. (b) Equivalent circuit.

The rest of this article is organized as follows. Section II presents the procedure for determining electrical parameters. In Section III, the procedure for determining the mechanical parameters is described. In Section IV, the results of the simulation considering the determined electrical and mechanical parameters are presented. Furthermore, the results of the conducted tests are compared with those of the simulation, as described in Section IV. Finally, section Vconcludes this article.

II. Determination of Electrical Parameters Based on Experiments

Generally, a brushed dc motor is used in the throttle valve owing to its wide operating range and simple controllability. The brushed dc motor consists of a stator, rotor, brush, and commutator, as shown in Fig. 2. The stator is composed of permanent magnets with two poles. The rotor is composed of an armature coil with seven slots. The brush is composed of graphite, and the commutator is a copper structure connected to the armature coil. The brush and commutator are in contact with each other and deliver a constant current to the armature coil. The combined structure of the brush and commutator is shown in Fig. 3(a). A brush contact resistance is generated because the brush is attached to the commutator by the spring. Fig. 3(b) shows the equivalent circuit of the brushed dc motor. A voltage equation and motor torque can be

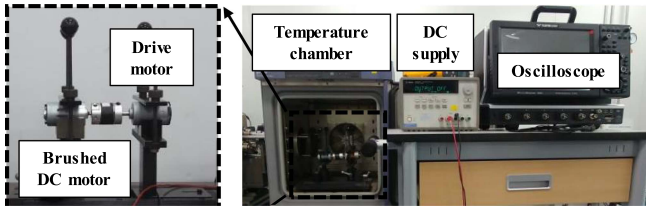

Fig. 4. Equipment for estimating electrical parameter.

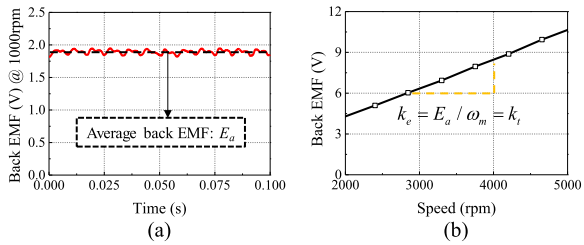

Fig. 5. Results of back EMF (a) obtained through no-load test at 1000 r/min and (b) constant.

expressed as

$$V_a = I_a R + E_a = I_a (R_a + R_b) + E_a \tag{1}$$

$$T_m = I_a k_t \tag{2}$$

where V_a and I_a are the input voltage and current, respectively. E_a is the back electromotive force (EMF). T_m and ω_m are the brushed dc motor torque and speed, respectively. The electrical parameters R, k_e, and k_t represent the total resistance, back EMF constant, and torque constant, respectively. The total resistance can be divided into the armature and brush contact resistances. R_a and R_b are the armature and brush contact resistances, respectively. The brush contact resistance is defined as a nonlinear parameter because the effective contact area between the brush and commutator depends on the input current and speed of rotation of the commutator. The electrical parameters that remain unaffected by the contact status of the brush are defined as linear parameters. These parameters include the back EMF constant, torque constant, and armature resistance.

A. Back EMF and Torque Constant

The back EMF constant is the ratio of the back EMF to the speed. As the back EMF constant and the torque constant are the same in the brushed dc motor, both parameters can be calculated using the no-load test. The test results of the magnitude and angular velocity of the back EMF are required to calculate the back EMF constant. The equipment used for the no-load test is shown in Fig. 4. While the brushed dc motor is rotated by the drive motor, the back EMF and the rotating speed are measured. The waveform of the back EMF measured at 1000 r/min is shown in Fig. 5(a). The magnitude of the back EMF in this figure is the average value of the measured back EMF. The angular velocity is determined by measuring the speed of the motor shaft. The ratio of the back EMF to the speed is calculated as the back EMF constant. The results for the back EMF constant are shown in Fig. 5(b). The torque constant can be calculated using the back EMF constant.

B. Armature Resistance

When the brushed dc motor is operated, the number of commutator segments connected to the brush differs according to the rotor position.

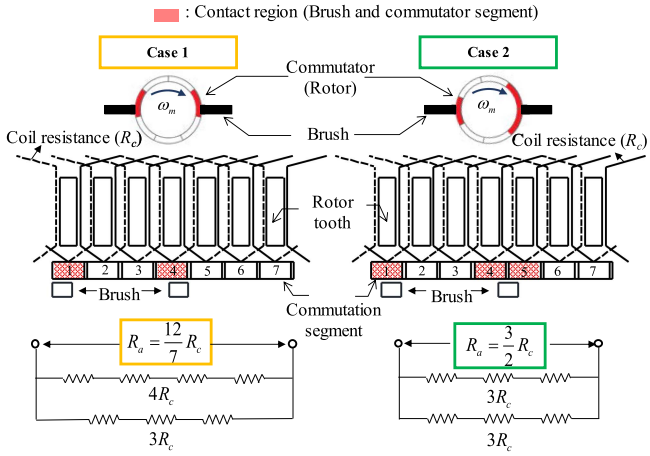

Fig. 6. Calculation of armature resistance considering rotor position.

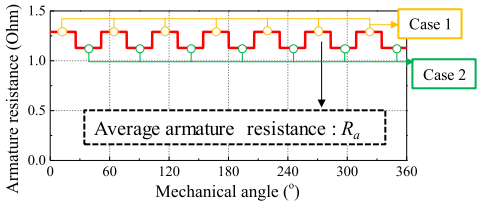

Fig. 7. Result of armature resistance.

Accordingly, the number of coils in a parallel circuit and the armature resistance vary with the rotor position. Fig. 6 illustrates the different rotor positions and the armature resistances in Cases 1 and 2. Lap winding is used as the winding method for the coil. Each rotor tooth is wound with the same number of coil turns. The coil resistance in one tooth is defined as

$$R_c = \rho\,(l/S) \tag{3}$$

where l and S are the length and area of the coil conductor, respectively. ρ is resistivity. When two commutator segments contact the brush in Case 1, the armature resistance consists of parallel circuits in the coil resistances of the four series and coil resistances of the three series. When three commutator segments contact the brush in Case 2, the armature resistance consists of parallel circuits in the coil resistances of the three series. Fig. 7 shows the armature resistance according to the rotor position. The armature resistance in Case 1 is the largest, and that in Case 2 is the smallest. In addition, depending on the rotor position, Cases 1 and 2 are repeated for the number of commutation segments. Thus, the armature resistance is calculated as the average of the resistances of Cases 1 and 2.

C. Brush Contact Resistance

The brush contact resistance is generated owing to the contact between the brush and commutator. As the contact area between the brush and commutator varies with the input current and rotor speed, the brush contact resistance is affected by the load. Furthermore, calculating the brush contact resistance using a mathematical equation is difficult, it is indirectly estimated using the voltage, current, and speed obtained from the load test. The voltage equation is used to calculate the brush

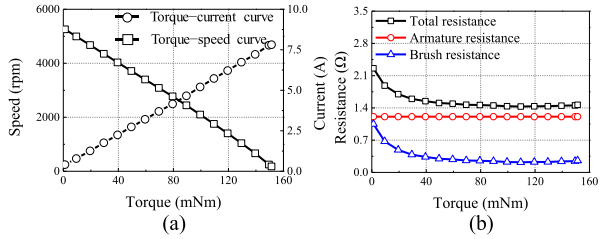

Fig. 8. Results (a) load test and (b) corresponding brush contact resistance.

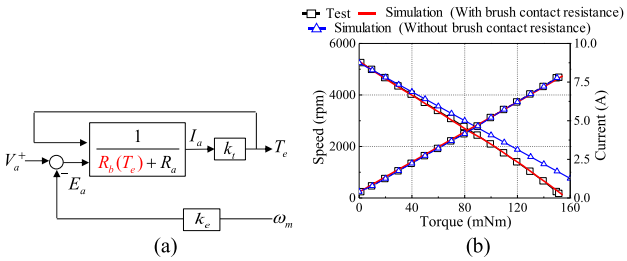

Fig. 9. Model of brushed dc motor considering brush effect (a) Block diagram and (b) Comparison between simulation and test results.

contact resistance is obtained as follows:

$$R_b = \frac{V_a - k_e\omega_m}{I_a} - R_a \tag{4}$$

To evaluate the brush contact resistance, a load test was performed using the equipment shown in Fig. 4. Fig. 8(a) shows the load test results depending on the load torque. By substituting the load test results, the back EMF constant, and the armature resistance in (4), the brush contact resistance is calculated. The total, armature, and brush contact resistances according to the load torque are shown in Fig. 8(b). When the load torque is low, the motor speed is high, and the brush resistance increases. The armature resistance is not affected by the load. The total resistance is expressed as the sum of the armature and brush contact resistance.

Fig. 9 shows the difference in motor performance between the simulation and test results according to the brush contact resistance. The simulations and tests were conducted with the same input voltage and temperature conditions. Fig. 9(a) shows a block diagram for predicting the performance of a brushed dc motor. The test and simulation results based on the brush contact resistance are shown in Fig. 9(b). If the brush contact resistance is excluded, the error between the simulation and test results increases according to the load torque. Therefore, the accuracy of the mathematical model can be improved by including the brush contact resistance.

III. Determination of Mechanical Parameters Based on Experiments

The mechanical components of the throttle valve include gears, a plate, and springs, as shown in Fig. 1. The mechanical parameters of the throttle valve include the friction coefficient, moment of inertia, and spring constant. Theoretically, the mechanical parameters are difficult to calculate because of the complex shape of the gears, motor, and plate. Therefore, the mechanical parameters are calculated through an experiment. First, the friction coefficient and moment of inertia are calculated by considering the gears, motor, and plate without the spring. Next, the spring constant is calculated without the motor, plate, or gears.

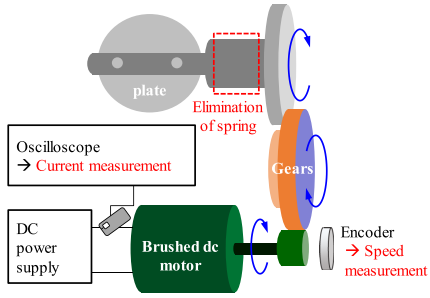

Fig. 10. Equipment for evaluating the friction coefficient and moment of inertia.

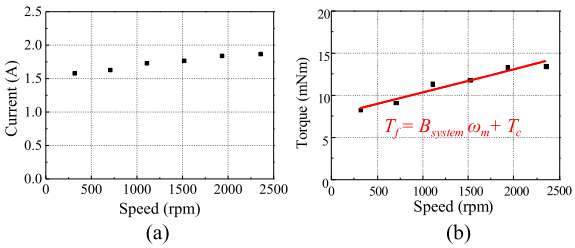

Fig. 11. Process for calculating the friction coefficient (a) speed–current and (b) speed–torque.

A. Friction Coefficient

The friction torque is expressed as

$$T_f = B_{\text{system}}\omega_m + T_c \tag{5}$$

where B_{system} is the friction coefficient for throttle valve system. T_c is the load torque of Coulomb friction. Fig. 10 shows the equipment used to estimate the friction coefficient. The speed was measured using an encoder installed on the motor shaft. The torque is indirectly measured using the motor current instead of using a torque sensor. Fig. 11(a) shows the measurement results of the current depending on the speed. The torque is calculated from the current supplied to the motor by using (2). The current at each speed is determined and converted into torque to calculate the friction coefficient. Fig. 11(b) shows the speed–torque curve for the case, where the current is converted into torque. The slope of the speed–torque curve represents the friction coefficient, and the intercept is calculated as the load torque of the Coulomb friction.

B. Moment of Inertia

The relationship between the speed and mechanical time constant can be formulated using the following motion equation:

$$J_{\text{system}} = -B_{\text{system}}t/\ln(\omega_m/\omega_{mo}) \tag{6}$$

where ω_{mo} is the initial speed, and t is the time. J_{system} is the moments of inertia of throttle valve system. The equipment used to evaluate the moment of inertia is shown in Fig. 10. As the moment of inertia is calculated from the transient section of the motor shaft speed, the motion of the motor is implemented based on the motor drive. As shown in Fig. 12, the speed of the motor shaft is measured as a function of time. The speed in the deceleration section is determined by the moment of inertia and the friction coefficient. Therefore, the moment of inertia is calculated using (6), along with the time and speed of the cut-off power in the deceleration section.

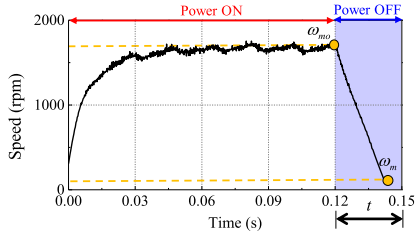

Fig. 12. Calculation for the moment of inertia.

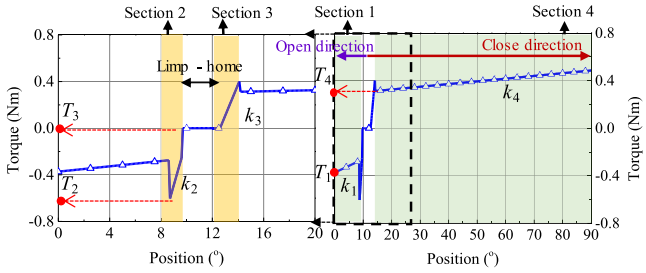

Fig. 13. Calculation for spring constant.

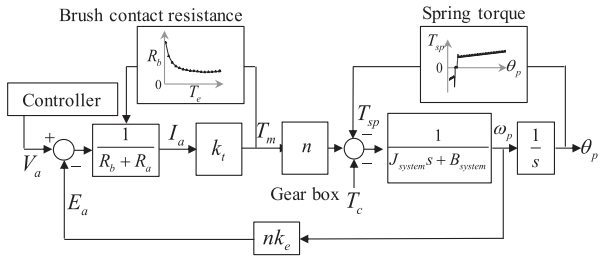

Fig. 14. Block diagram considering nonlinear electrical and mechanical parameters.

C. Spring Constant

The spring inserted into the plate is shown in Fig. 1. Two springs are installed on the plate to assist with the opening or closing of the plate. The two springs located in the throttle valve have different rolling directions and numbers of turns. The balance of the forces generated by the two springs is the limp-home. The spring torque is evaluated using a device that can measure the torque according to the plate position. The measurements of the actual spring torque are presented in Fig. 13. Sections I and II indicate the angle range in the closing direction, and Sections III and IV indicate the angle range in the opening direction. The characteristics of the torque differ depending on the section. Therefore, the spring constant and the load torque of the spring are divided into four sections and calculated as

$$T_{sp}(\theta) = \left\{ \begin{array}{l} k_1\theta + T_1 \text{ if Section 1}, \; k_2\theta + T_2 \text{ if Section 2} \\ k_3\theta + T_3 \text{ if Section 3}, \; k_4\theta + T_4 \text{ if Section 4} \end{array} \right\} \tag{7}$$

where k_1–k_4 represent the spring constants, and T_1–T_4 represent the load torques of the spring for each section. The load torque of the spring is determined using the y-intercept generated in each section.

IV. Verification of Simulation and Experiment

Fig. 14 shows the block diagram considering nonlinear parameters. The simulation results were compared with the test results to verify the constructed block diagram. Fig. 15 shows the equipment used to compare the simulation and test results. First, simulations and tests

Fig. 15. Equipment for simulation and test verification.

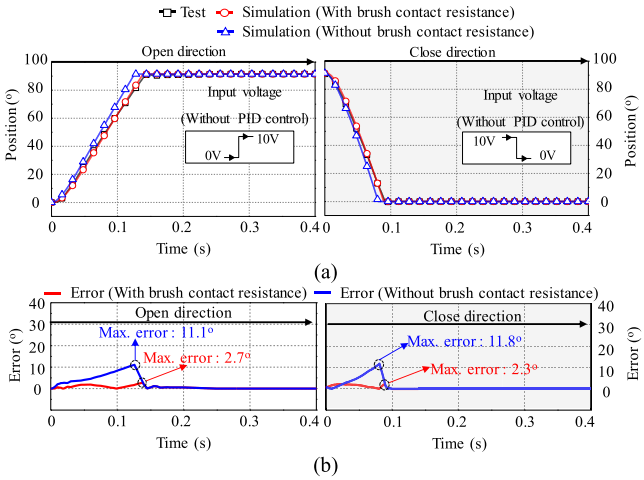

Fig. 16. Comparison of simulation and test results without PID control (a) plate motion and (b) error.

were conducted without a controller. Next, an appropriate PID gain that satisfied the target performance was selected and reflected in the controller when performing the test. Subsequently, the simulation and test results were compared under the same PID gain and conditions.

A. Dynamic Characteristic Without PID Controller

Fig. 16 shows the simulation and test results for the plate motion of the throttle valve when a step voltage is applied without PID control. In particular, the simulation was performed by throttle valve modeling according to the brush contact resistance as a nonlinearity parameter, as shown in Fig. 16(a). The plate motion was determined based on the electrical and mechanical parameters. Therefore, by applying a step voltage, the estimated electrical and mechanical parameters could be verified through errors between the simulation and test results. The error was calculated to the difference between the plate angles of the simulation and test, as shown in Fig. 16(b). When brush contact resistance was not considered in the simulation, the maximum error between the simulation and test results was 11.8°. However, when the brush contact resistance was considered, the maximum error between the simulation and test results was 2.7°. These results suggest that the brush contact resistance needs to be considered in throttle valve modeling.

B. Dynamic Characteristic With PID Controller

Fig. 17 presents the simulation and test results obtained when considering PID control. The PID gain was appropriately selected such that the target performance of the throttle valve was achieved. When the reference voltage is applied from the controller, the plate motion of the throttle valve and the applied current of the motor are determined by the PID gain and parameters. Fig. 17(a) shows the simulation and test

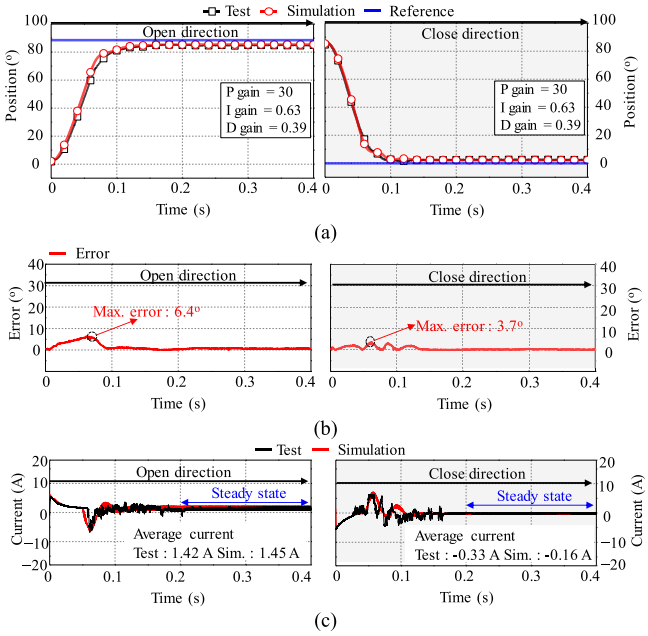

Fig. 17. Comparison of simulation and test results with PID control: (a) plate motion, (b) error, and (c) input current.

TABLE I
COMPARISON BETWEEN TEST AND SIMULATION RESULTS

		Simulation	Test
Opening direction	Rising time (ms)	84	82
	Maximum overshoot (°)	0.01	0.03
	Steady-state error (°)	3.83	3.58
Closing direction	Falling time (ms)	70	74
	Maximum overshoot (°)	0.36	0.3
	Steady-state error (°)	0.88	0.64

results of the plate motion. The error was calculated as the difference between the plate angles obtained from the simulation and the test. As shown in Fig. 17(b), the maximum error between the simulation and test results is 6.4°. Under a constant PID gain, the errors can increase owing to the nonlinear parameters in the transient section of the plate motion. The plate motion was evaluated using response time, overshoot, and steady-state error. A comparison of the simulation and test results is presented in Table I. Fig. 17(c) shows that the shapes of the average current and current waveforms in the steady-state are similar for the simulation and test results.

V. CONCLUSION

A parameter calculation method that considers not only the electrical nonlinearity, but also the mechanical nonlinearity was proposed in this article. In addition, throttle valve modeling using a mathematical block diagram was proposed considering the electrical and mechanical nonlinearities. Finally, the dynamic characteristics of the throttle valve with the PID control were confirmed as maximum overshoot, steady-state error, and response time. The proposed throttle valve modeling and calculated parameters were verified by comparing the simulation and test results in detail. In conclusion, the accuracy of throttle valve modeling was improved by considering both electrical and mechanical nonlinearity parameters. In future work, it will be necessary to study a control strategy that considers electrical as well as mechanical nonlinearity parameters based on PID control.

REFERENCES

[1] D. Kim, H. Peng, S. Bai, and J. M. Maguire, "Control of integrated powertrain with electronic throttle and automatic transmission," *IEEE Trans. Control Syst. Technol.*, vol. 15, no. 3, pp. 474–482, May 2007.

[2] Y. Pan, U. Ozguner, and O. H. Dagci, "Trends and future perspectives of electronic throttle control system in a park ignition engine," *Ann. Rev Control*, vol. 44, pp. 97–115, May 2017.

[3] Z. Quyang and W. Junli, "Nonlinear PID control of electronic throttle valve," in *Proc. IEEE Conf. Electron. Control Eng.*, Sep. 2011, pp. 722–724.

[4] J. Zheng, H. Wang, Z. Man, J. Jin, and M. Fu, "Robust motion control of a linear motor positioner using fast nonsingular terminal sliding mode," *IEEE/ASME Trans. Mechatron.*, vol. 20, no. 4, pp. 1743–1752, Aug. 2015.

[5] Y. Li, B. Yang, T. Zheng, Y. Li, M. Cui, and S. Peeta, "Extended-state-observer-base double-loop integral sliding-mode control of electronic throttle valve," *IEEE Trans. Int. Trans. Syst.*, vol. 16, no. 5, pp. 2501–2510, Oct. 2015.

[6] H. Wang *et al.*, "Adaptive integral terminal sliding mode control for automobile electronic throttle via an uncertainty observer and experimental validation," *IEEE Trans. Veh. Technol.*, vol. 67, no. 9, pp. 8129–8143, Sep. 2018.

[7] Y. Pan, U. Ozguner, and O. H. Dagci, "Variable-structure control of electronic throttle valve," *IEEE Trans. Ind. Electron.*, vol. 55, no. 11, pp. 3899–3907, Nov. 2008.

[8] C. Wang and D. Huang, "A new intelligent fuzzy controller for nonlinear hysteretic electronic throttle in modern intelligent automobiles," *IEEE Trans. Ind. Electron.*, vol. 60, no. 6, pp. 2332–2345, Jun. 2013.

[9] X. Jiao, J. Zhang, and T. Shen, "An adaptive servo control strategy for automotive electronic throttle and experimental validation," *IEEE Trans. Ind. Electron.*, vol. 61, no. 11, pp. 6275–6284, Nov. 2014.

[10] R. Grepl and B. Lee, "Modeling, parameter calculation and nonlinear control of automotive electronic throttle using a rapid-control prototyping technique," *Int. J. Autom. Technol.*, vol. 11, no. 4, pp. 601–610, Aug. 2010.

[11] M. Mcharek, T. Azib, M. Hammadi, C. Larouci, and J. Y. Choley, "Multiphysical design approach for automotive electronic throttle body," *IEEE Trans. Ind. Electron.*, vol. 67, no. 8, pp. 6752–6761, Aug. 2020.

[12] G. Sincero, J. Cros, and P. Viarouge, "Arc models for simulation of brush motor commutations," *IEEE Trans. Magn.*, vol. 44, no. 6, pp. 1518–1521, Jun. 2008.

[13] G. Mirzaeva, R. E. Betz, and T. J. Summers, "Evaluation of current density in DC motor brushes for mining machines based on air-gap field measurement," *IEEE Trans. Ind. Appl.*, vol. 46, no. 4, pp. 1255–1263, Jul. 2010.

[14] A. Di Gerlando and R. Perini, "Model of the commutation phenomena in a universal motor," *IEEE Trans. Energy Convers.*, vol. 21, no. 1, pp. 27–33, Mar. 2006.

[15] J. Deur, D. Pavkovic, N. Peric, M. Jansz, and D. Hrovat, "An electronic throttle control strategy including compensation of friction and limp-home effects," *IEEE Trans. Ind. Appl.*, vol. 40, no. 3, pp. 821–834, May/Jun. 2004.

[16] M. Ye and H. Wang, "A robust adaptive chattering-free sliding mode control strategy for automotive electronic throttle system via genetic algorithm," *IEEE Access*, vol. 8, pp. 68–80, 2020.